PREPARATION AND OPERATIONS OF THE MISSION PERFORMANCE CENTRE (MPC) FOR THE COPERNICUS SENTINEL-3 MISSION

S3-A SLSTR Cyclic Performance Report

Cycle No. 026

Start date: 20/12/2017

End date: 16/01/2018

SENTINEL 3

Mission Performance Centre

Ref.: S3MPC.RAL.PR.02-026
Issue: 1.0
Date: 22/01/2018
Contract: 4000111836/14/I-LG

Customer:	ESA	**Document Ref.:**	S3MPC.RAL.PR.02-026
Contract No.:	4000111836/14/I-LG	**Date:**	22/01/2018
		Issue:	1.0

Project:	PREPARATION AND OPERATIONS OF THE MISSION PERFORMANCE CENTRE (MPC) FOR THE COPERNICUS SENTINEL-3 MISSION		
Title:	S3-A SLSTR Cyclic Performance Report		
Author(s):	SLSTR ESLs		
Approved by:	D. Smith, SLSTR ESL Coordinator	**Authorized by**	Frédéric Rouffi, OPT Technical Performance Manager
Distribution:	ESA, EUMETSAT, S3MPC consortium		
Accepted by ESA	S. Dransfeld, MPC Deputy TO for OPT P. Féménias, MPC TO		
Filename	S3MPC.RAL.PR.02-026 - i1r0 - SLSTR Cyclic Report 026.docx		

Changes Log

Version	Date	Changes
1.0	22/01/2018	First Version

List of Changes

Version	Section	Answers to RID	Changes

Table of content

List of Figures

List of Tables

1 Processing Baseline Version

IPF	IPF / Processing Baseline version	Date of deployment
SL1	06.14 / 2.17	CGS: 05/07/2017 13:15 UTC (NRT) PAC: 05/07/2017 12:34 UTC (NTC)
SL2	06.12 / 2.17	CGS: 05/07/2017 13:16 UTC (NRT) PAC: 05/07/2017 12:42 UTC (NTC)

2 Instrument monitoring

2.1 Instrument temperatures

- Instrument temperatures were stable and consistent with expected values following the decontamination phase which was performed towards the end of Cycle 20 (see Figure 1).
- Figure 2, Figure 4 and Figure 5 show the orbital average blackbody, baffle and OME temperatures during cycle 26. The temperatures were stable (on top of a daily variation cycle). Longer term analysis also shows a yearly variation, with temperatures rising as the Earth approaches perihelion at the beginning of January. Cycle 26 falls at this yearly peak with +YBB temperatures around 304 K (see Figure 3 and Table 3). Figure 2 shows that gradients across the blackbody baseplate are stable and within their expected range (±20mK).

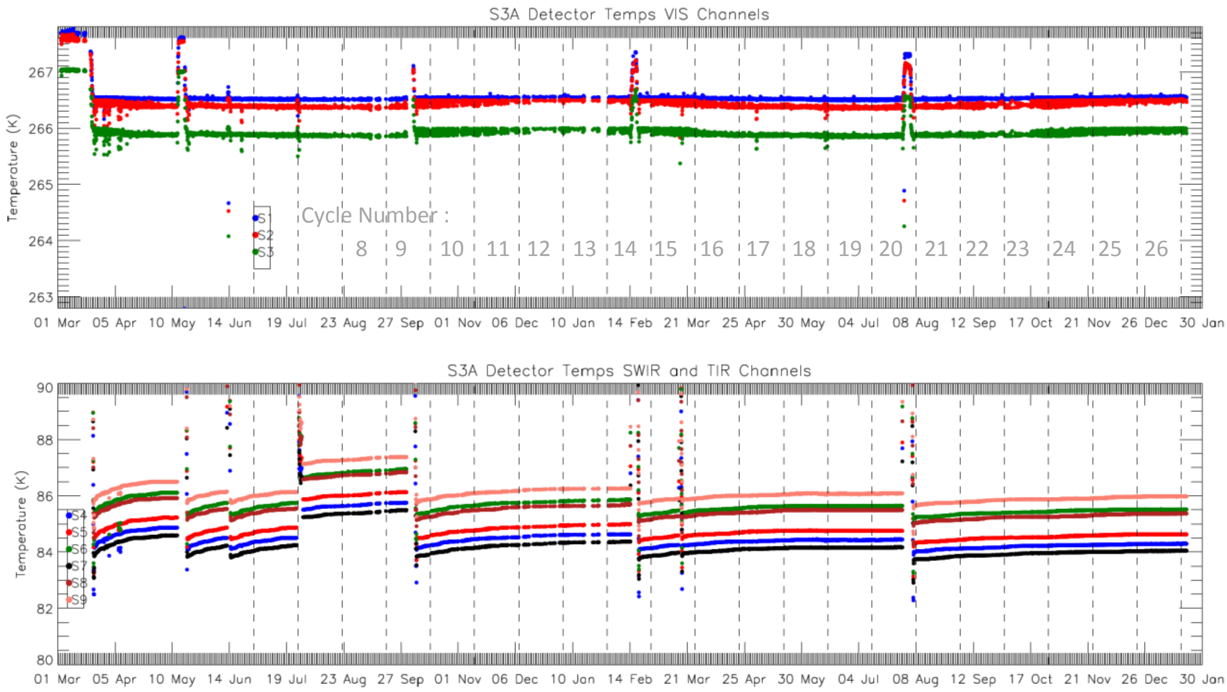

Figure 1: Detector temperatures for each channel from 1st March 2016. Discontinuities occur for the infrared channels where the FPA was heated for decontamination or following an anomaly. The vertical dashed lines indicate the start and end of each cycle. Each dot represents the average temperature in one orbit.

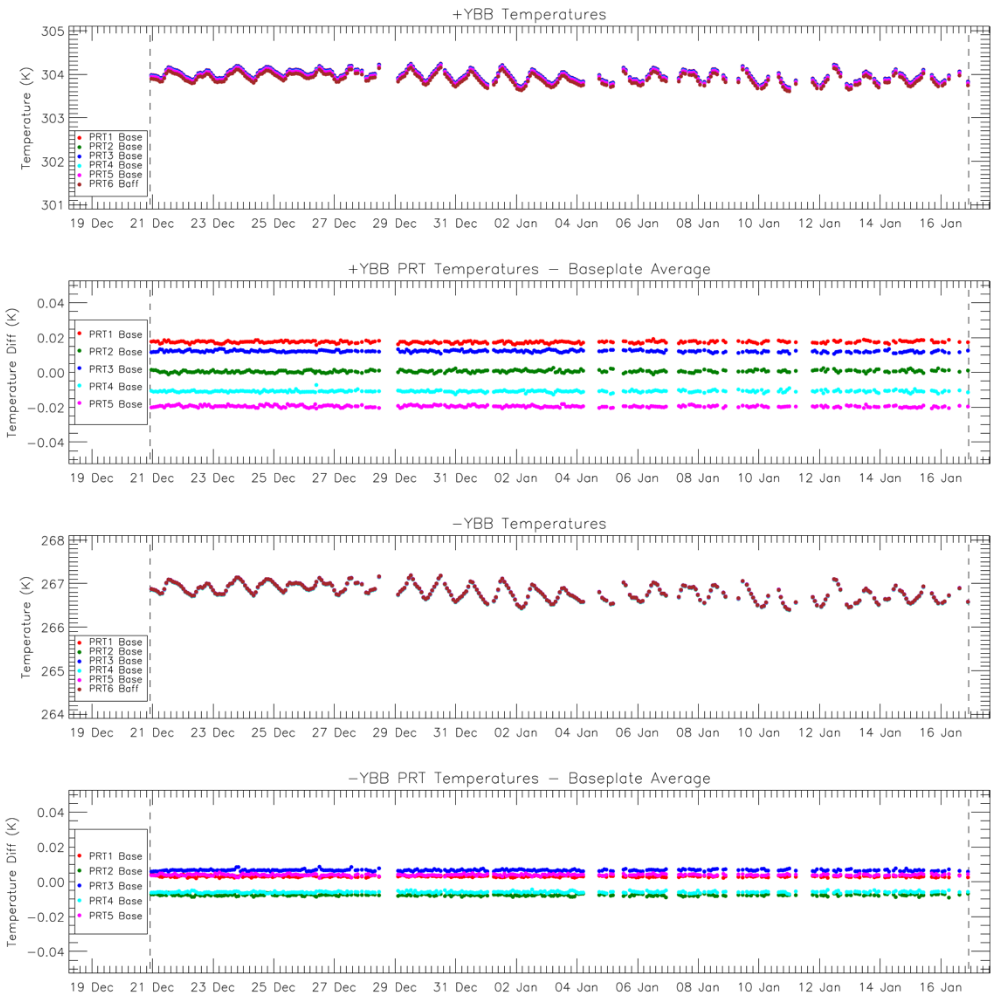

Figure 2: Blackbody temperature and baseplate gradient trends during cycle 26. The vertical dashed lines indicate the start and end of the cycle. Each dot represents the average temperature in one orbit. Note that the gaps are in the stream of data from the MPC used for monitoring, and are not due to any problem.

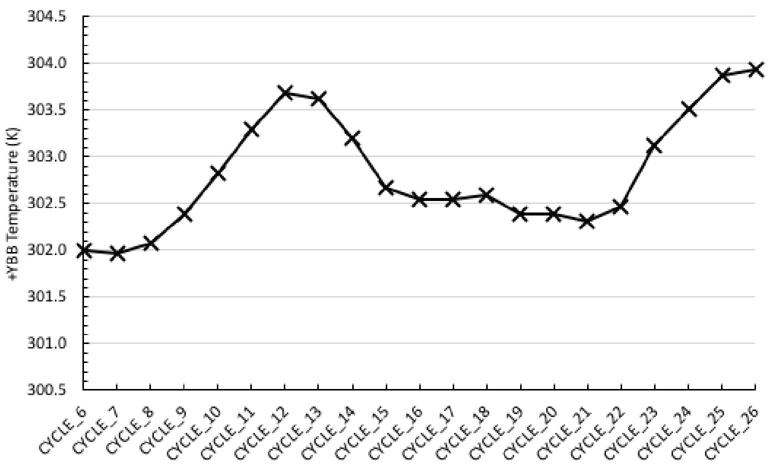

Figure 3: Long term trends in average +YBB temperature in each cycle, showing yearly variation.

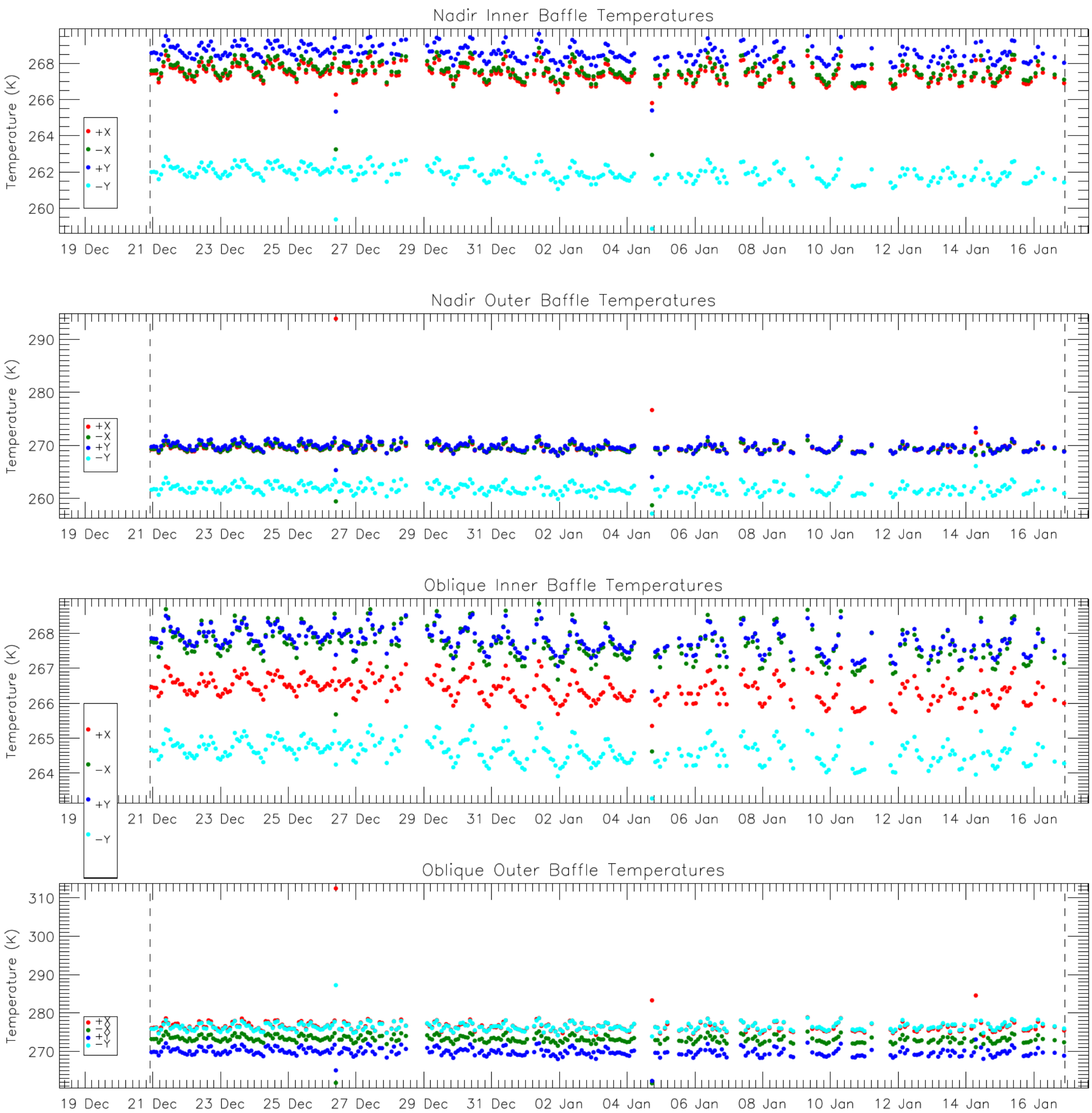

Figure 4: Baffle temperature trends for cycle 26. The vertical dashed lines indicate the start and end of the cycle. Each dot represents the average temperature in one orbit.

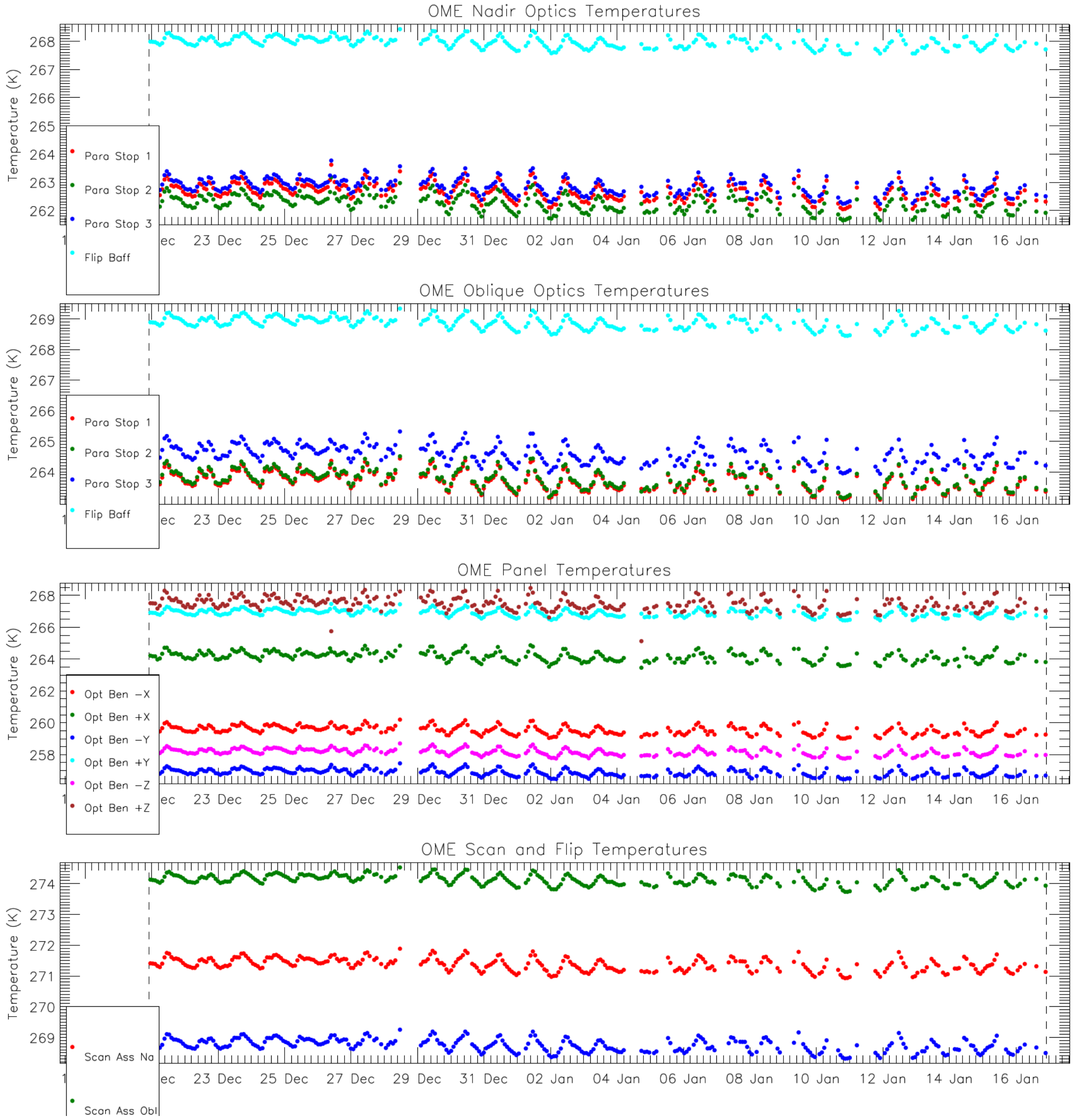

Figure 5: Opto-Mechanical Enclosure (OME) temperature trends for cycle 26 showing the paraboloid stops and flip baffle (top two plots) and optical bench and scanner and flip assembly (lower two plots). The vertical dashed lines indicate the start and end of the cycle. Each dot represents the average temperature in one orbit.

2.2 Scanner performance

Scanner performance in cycle 26 has been consistent with previous operations and within required limits.

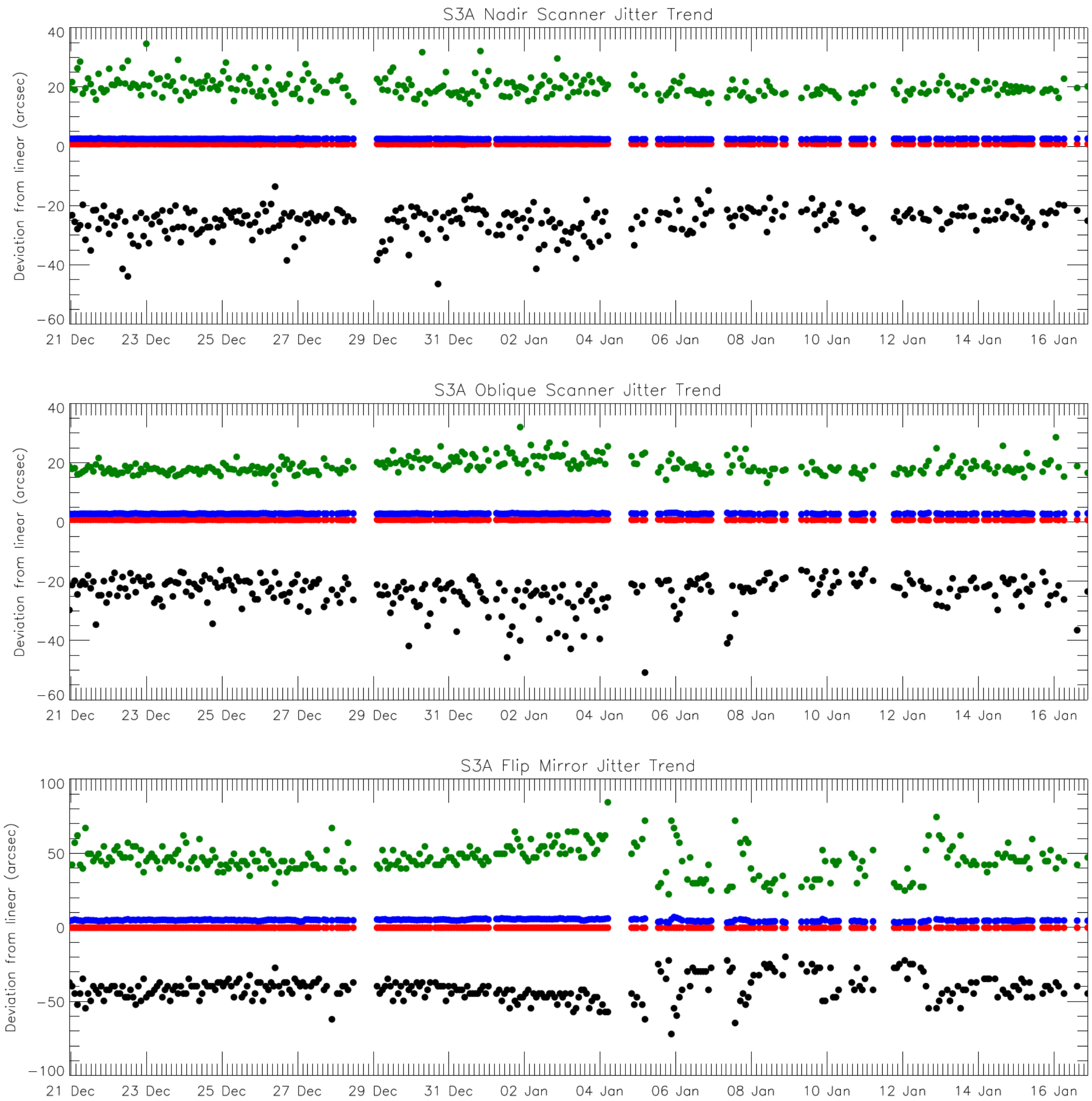

Figure 6: Scanner and flip jitter for cycle 26, showing mean, stddev and max/min position per orbit compared to the expected one for the nadir view.

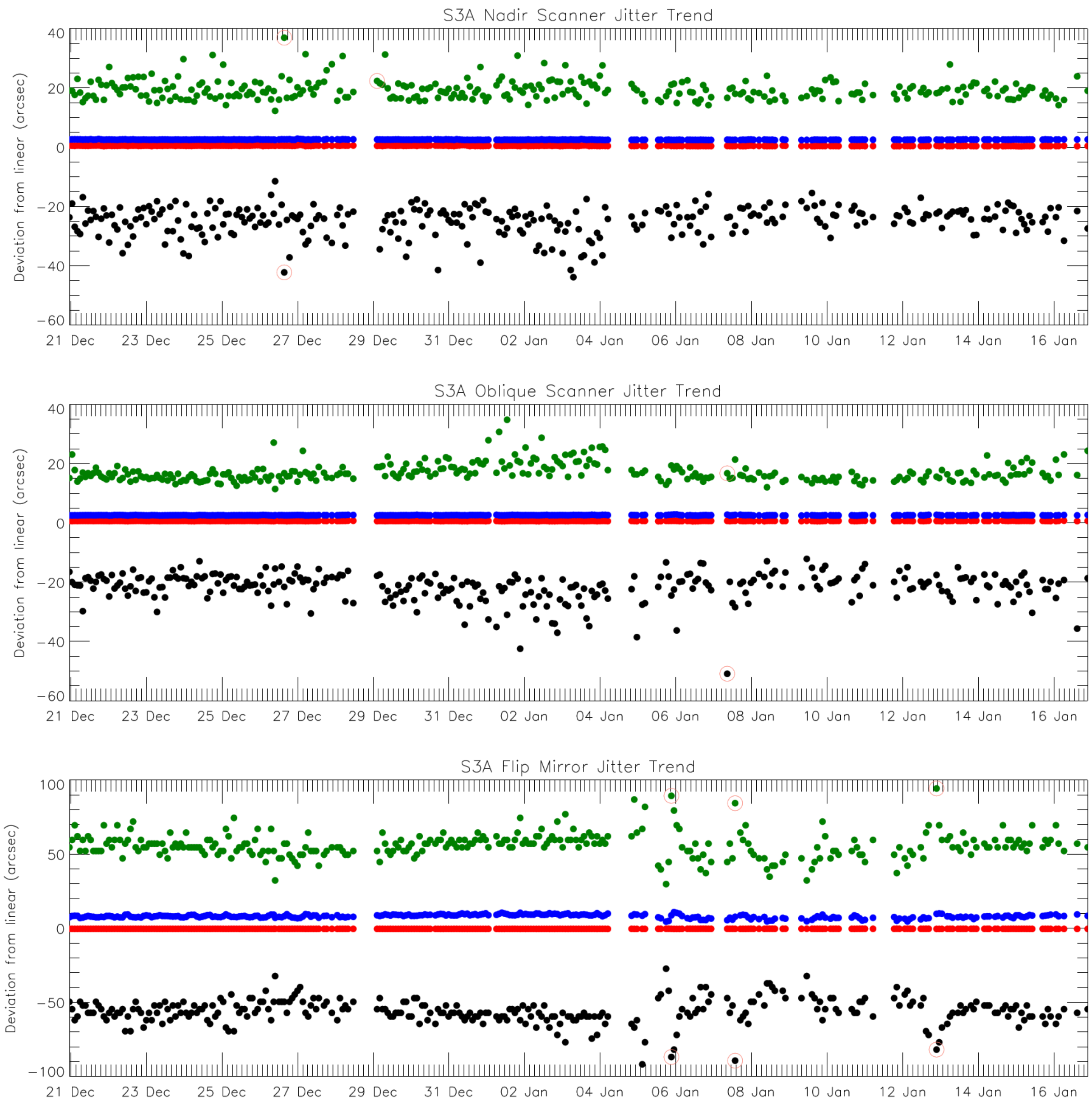

Figure 7: Scanner and flip jitter for cycle 26, showing mean, stddev and max/min position per orbit compared to the expected one for the oblique view.

2.3 Detector noise levels

2.3.1 VIS and SWIR channel signal-to-noise

The VIS and SWIR channel noise in cycle 26 was stable and consistent with previous operations - the signal-to-noise ratio of the measured VISCAL signal over the mission so far is plotted in Figure 8. Table 1 and Table 2 give the average signal-to-noise in each cycle (excluding the anomaly/decontamination period in Cycle 20). Note that this averages over the significant detector-detector dispersion for the SWIR channels that is shown in Figure 8.

Table 1: Average reflectance factor, and signal-to-noise ratio of the measured VISCAL signal for cycles 015-026, averaged over all detectors for the nadir view.

	Average Reflectance Factor	Nadir Signal-to-noise ratio											
		Cycle 015	Cycle 016	Cycle 017	Cycle 018	Cycle 019	Cycle 020	Cycle 021	Cycle 022	Cycle 023	Cycle 024	Cycle 025	Cycle 026
S1	0.187	224	233	234	231	230	232	230	232	234	235	234	278
S2	0.194	230	236	236	232	231	235	235	235	239	236	237	233
S3	0.190	230	236	238	228	231	229	231	229	234	232	234	227
S4	0.191	139	142	140	140	139	137	135	136	139	140	142	141
S5	0.193	233	233	235	236	234	232	232	229	236	236	235	238
S6	0.175	144	142	143	143	142	139	138	139	142	146	145	146

Table 2: Average reflectance factor, and signal-to-noise ratio of the measured VISCAL signal for cycles 015-026, averaged over all detectors for the oblique view.

	Average Reflectance Factor	Oblique Signal-to-noise ratio											
		Cycle 015	Cycle 016	Cycle 017	Cycle 018	Cycle 019	Cycle 020	Cycle 021	Cycle 022	Cycle 023	Cycle 024	Cycle 025	Cycle 026
S1	0.166	236	243	247	246	242	240	240	241	243	246	246	239
S2	0.170	241	248	251	249	247	246	245	246	253	249	251	243
S3	0.168	236	245	249	244	242	238	238	238	247	239	244	234
S4	0.166	108	108	111	110	109	108	108	108	110	111	111	110
S5	0.166	172	169	169	171	168	167	168	168	172	173	173	172
S6	0.155	107	109	109	110	108	106	108	107	111	110	113	109

Note that there may be very small differences in the average signal-to-noise values in Table 1 and Table 2 for recent cycles compared to previous Cyclic Reports because additional products may have been received from the MPC since those reports were published.

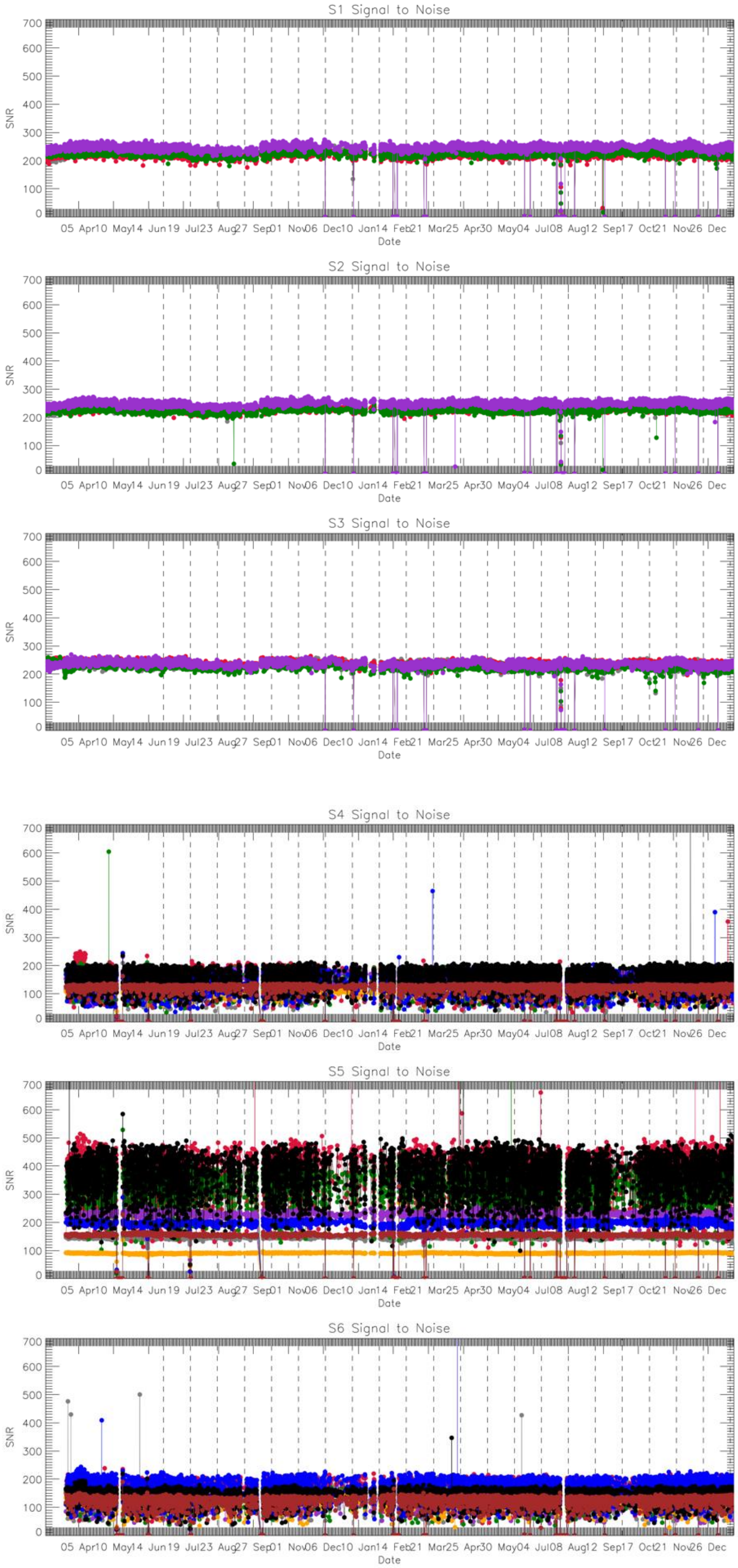

Figure 8: VIS and SWIR channel signal-to-noise of the measured VISCAL signal in each orbit. Different colours indicate different detectors.

2.3.2 TIR channel NEDT

The thermal channel NEDT values in cycle 26 are consistent with previous operations and within the requirements. NEDT values for each cycle, averaged over all detectors and both Earth views, are shown in Table 3 and Table 4.

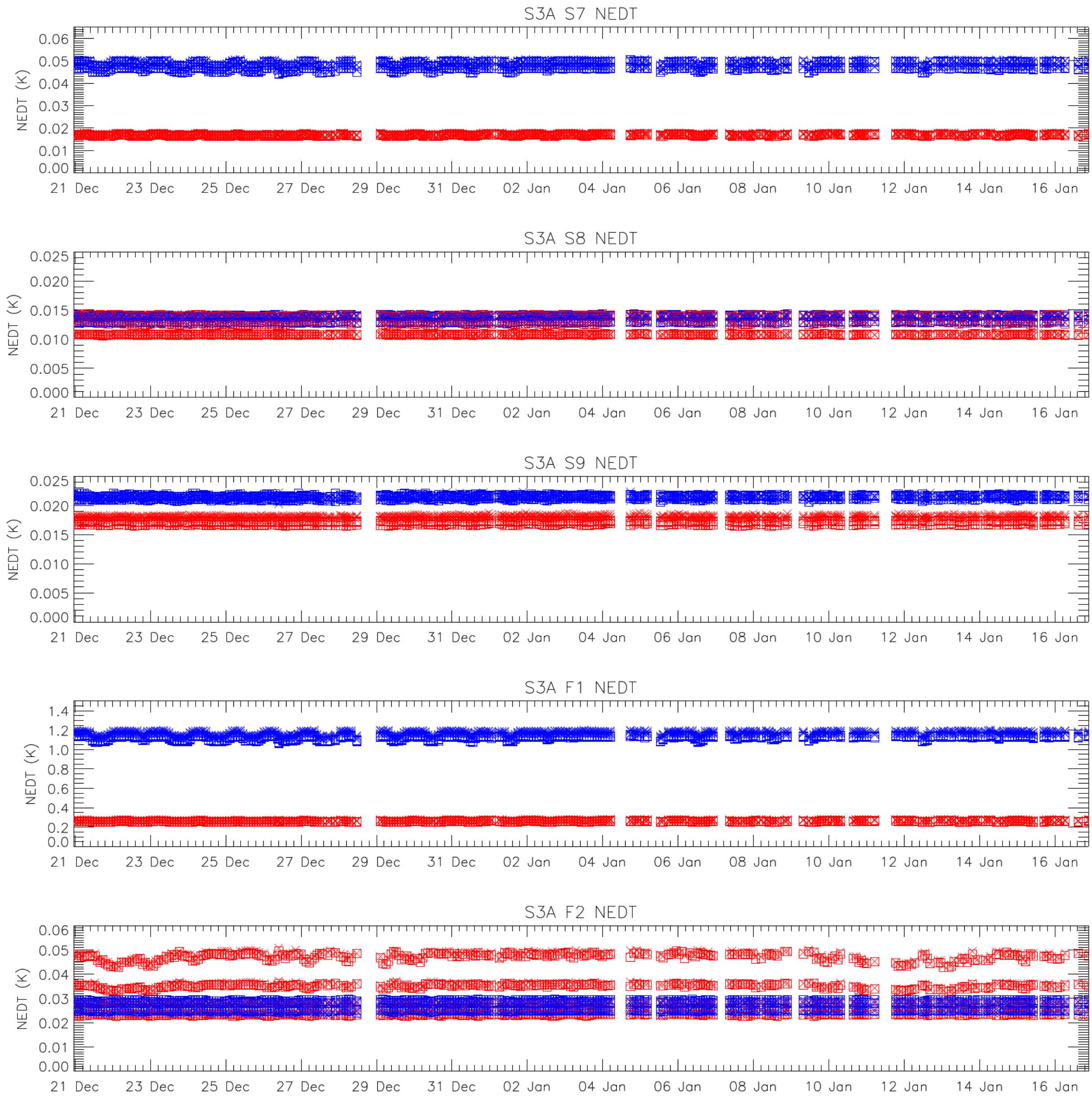

Figure 9: NEDT trend for the thermal channels in cycle 26. Blue points were calculated from the cold blackbody signal and red points from the hot blackbody. The square symbols show results calculated from the nadir view and crosses show results from the oblique view. Results are plotted for all detectors and integrators, which is why there are several different levels within the same colour points (particularly for S8 and F2).

Table 3: NEDT for cycles 015-026 averaged over all detectors for both Earth views towards the +YBB (hot).

		Cycle 015	Cycle 016	Cycle 017	Cycle 018	Cycle 019	Cycle 020	Cycle 021	Cycle 022	Cycle 023	Cycle 024	Cycle 025	Cycle 026
+YBB temp (K)		302.674	302.544	302.541	302.593	302.385	302.395	302.316	302.466	303.125	303.515	303.871	303.931
NEDT (mK)	S7	16.9	17.2	17.2	18.1	17.2	17.2	17.1	17.2	16.9	16.8	16.7	16.7
	S8	11.0	10.9	11.0	11.1	11.0	11.1	10.9	10.9	10.9	10.8	10.8	10.8
	S9	17.6	17.0	17.2	17.5	17.4	17.5	16.7	16.9	17.0	17.1	17.1	17.2
	F1	260	268	271	297	276	276	269	270	265	265	263	263
	F2	27.9	27.6	27.8	27.8	27.8	27.8	27.4	27.6	27.7	27.9	28.0	27.9

Table 4: NEDT for cycles 015-026 averaged over all detectors for both Earth views towards the –YBB (cold).

		Cycle 015	Cycle 016	Cycle 017	Cycle 018	Cycle 019	Cycle 020	Cycle 021	Cycle 022	Cycle 023	Cycle 024	Cycle 025	Cycle 026
-YBB temp (K)		265.183	265.136	265.260	265.412	265.122	265.054	264.900	265.012	265.790	266.251	266.754	266.760
NEDT (mK)	S7	48.7	49.0	48.8	46.9	49.2	49.4	49.4	49.0	47.6	47.0	46.3	46.3
	S8	14.2	14.2	14.3	14.2	14.3	14.4	14.2	14.1	14.2	14.1	14.0	14.1
	S9	21.3	21.4	21.6	21.6	22.0	22.0	21.1	21.3	21.4	21.4	21.5	21.6
	F1	1222	1191	1199	1163	1231	1233	1212	1202	1161	1139	1124	1123
	F2	29.2	29.3	29.3	29.4	29.6	29.7	29.2	29.2	29.3	29.3	29.2	29.3

Note that there may be very small differences in the average NEDT values in Table 3 and Table 4 for recent cycles compared to previous Cyclic Reports because additional products may have been received from the MPC since those reports were published.

2.4 Calibration factors

2.4.1 VIS and SWIR VISCAL signal response

Signals from the VISCAL source for the VIS channels show oscillations due to the build up of ice on the optical path within the FPA. Decontamination must be carried out periodically in order to warm up the FPA and remove the ice. The latest decontamination cycle was successfully performed at the end of Cycle 20. The VISCAL signal has behaved as expected following the decontamination.

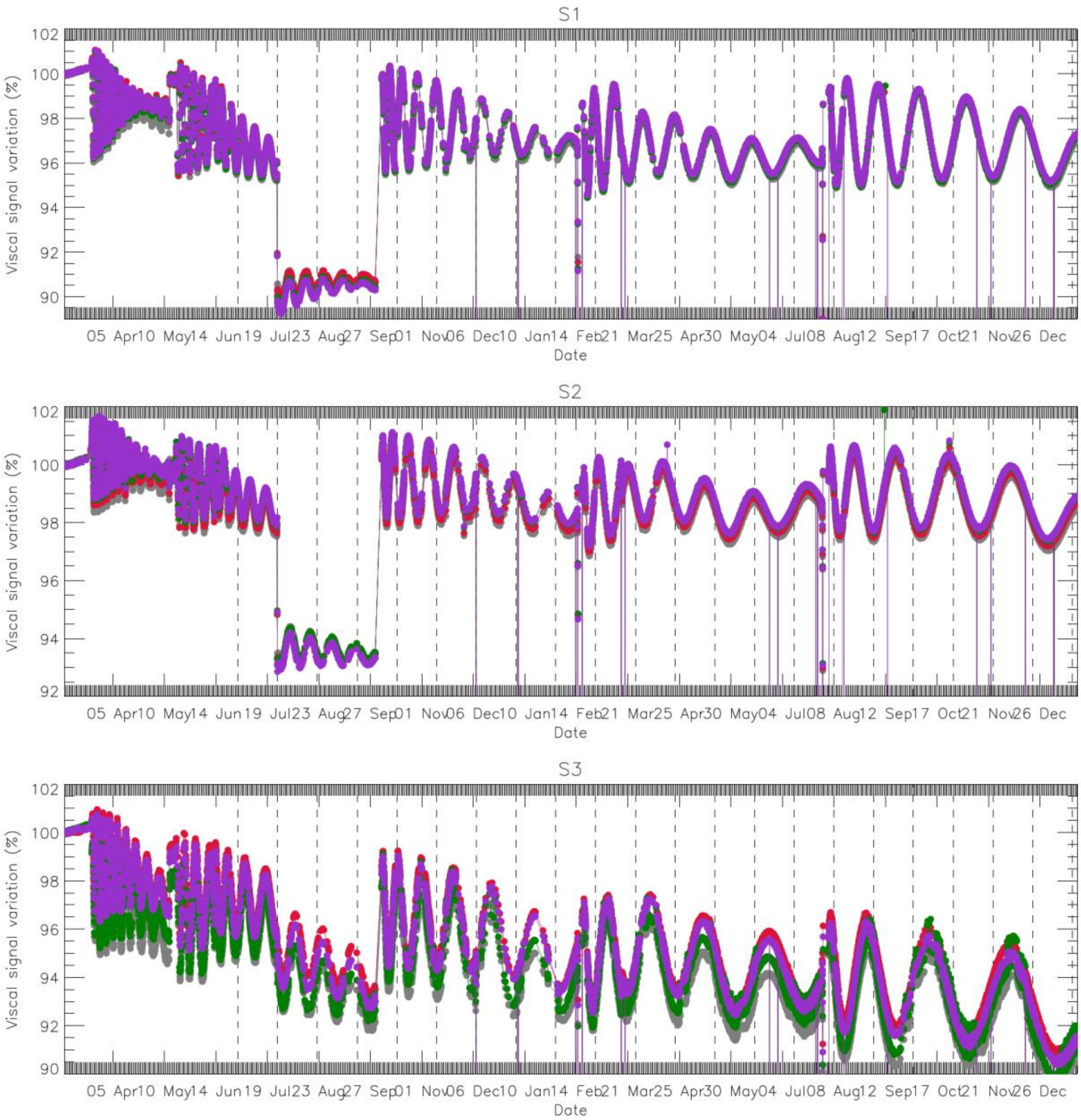

Figure 10: VISCAL signal trend for VIS channels (nadir view).

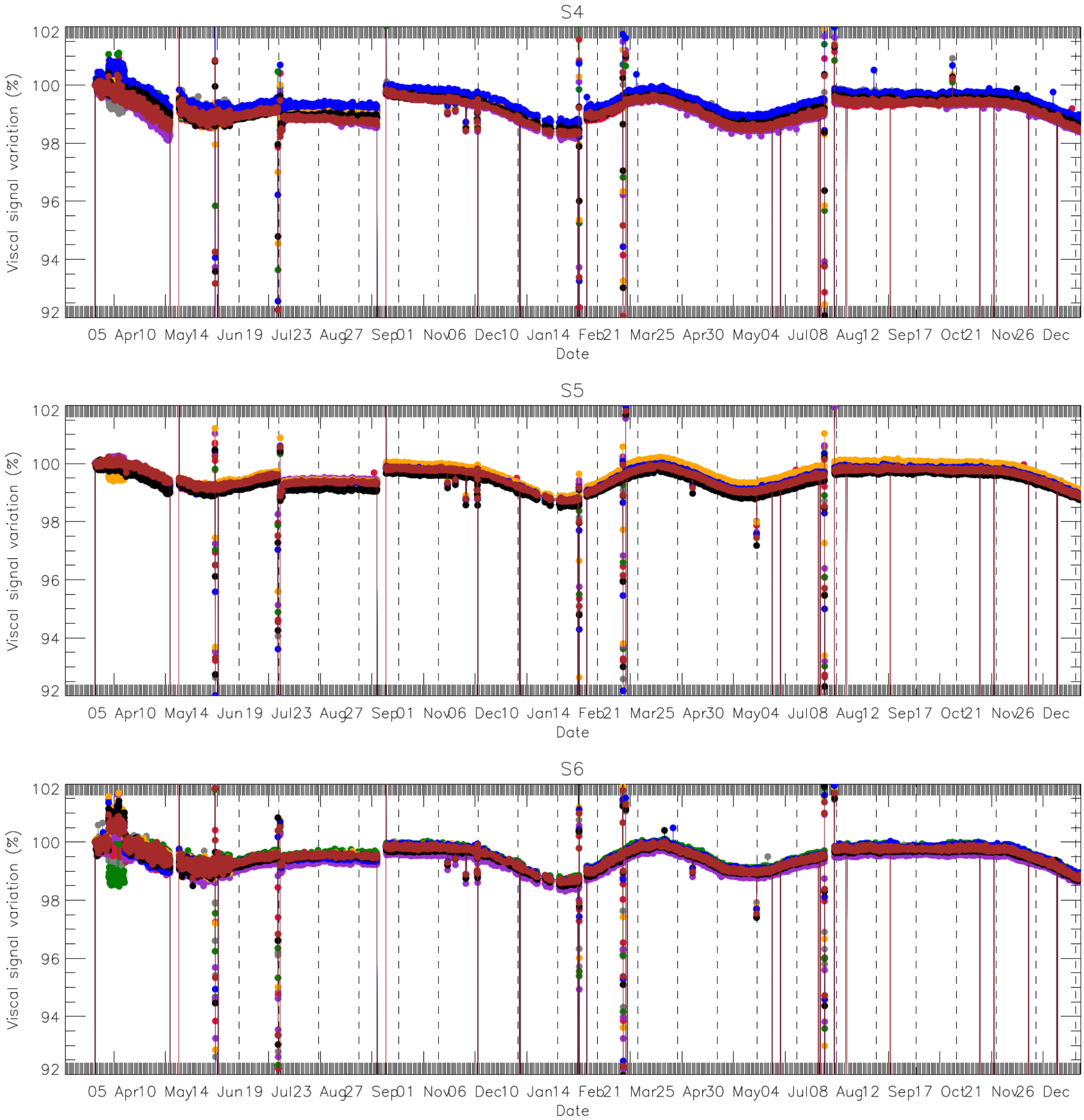

Figure 11: VISCAL signal trend for SWIR channels (nadir view).

3 Level-1 product validation

3.1 Geometric calibration/validation

Regular monitoring using the GeoCal Tool implemented at the MPC is being carried out. This monitors the geolocation performance in Level-1 images by correlation with ground control point (GCP) imagettes. Each Level-1 granule typically contains several hundred GCPs, which are filtered based on signal-to-noise to obtain a daily average in the across and along track directions. Results from the GeoCal Tool are currently being analysed and will be presented in future cyclic reports.

3.2 Radiometric validation

The radiometric calibration of the visible and SWIR channels is monitored using the S3ETRAC service. The S3ETRAC service extracts OLCI and SLSTR Level-1 data and computes associated statistics over 49 sites corresponding to different surface types (desert, snow, ocean maximising Rayleigh signal, and ocean maximising sunglint scattering). These S3ETRAC products are used for the assessment and monitoring of the VIS and SWIR radiometry by the ESL.

Details of the S3ETRAC/SLSTR statistics are provided on the S3ETRAC website http://s3etrac.acri.fr/index.php?action=generalstatistics#pageSLSTR

- Number of SLSTR products processed by the S3ETRAC service
- Statistics per type of target (DESERT, SNOW, RAYLEIGH, SUNGLINT)
- Statistics per site
- Statistics on the number of records

Analysis of S3ETRAC results for SLSTR radiometric validation is ongoing and will be presented in future cyclic reports.

3.3 Image quality

The Level-1 image quality is assessed when data are available at the MPC. For example by combining all granules over one day into a single Level-3 image. Figure 12 shows an example Level-3 image for the visible channels from 3rd January 2018 (daytime only).

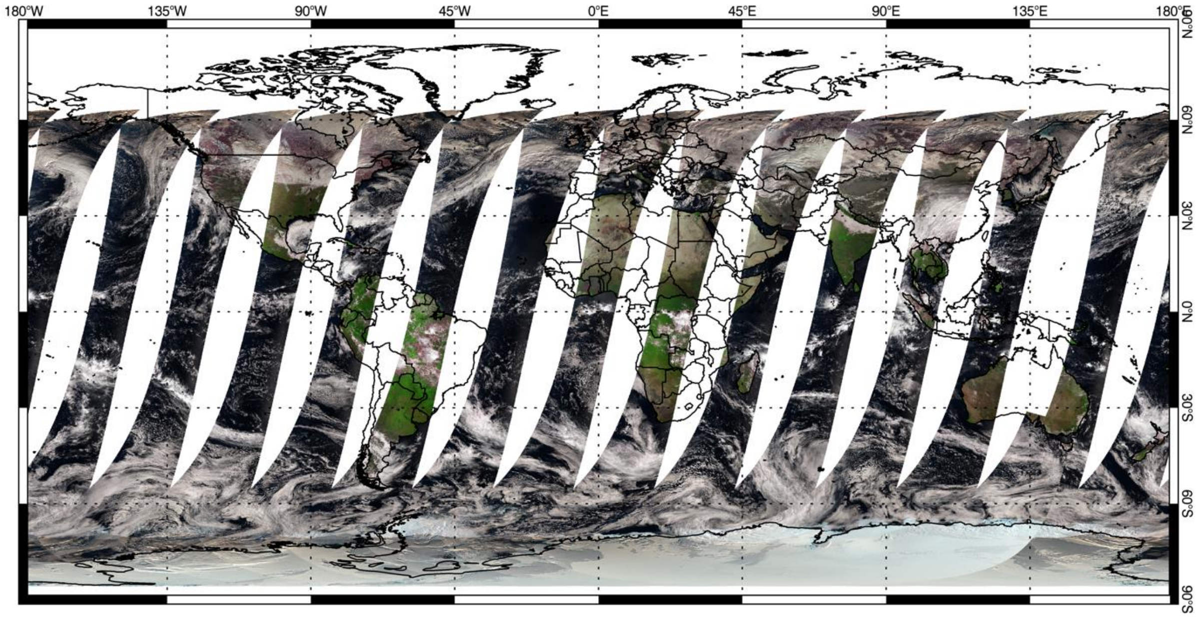

Figure 12: Daytime Level-3 image for visible channels on 3rd January 2018.

4 Level 2 SST validation

Level 2 WCT SSTs have been validated using CMEMS *in situ* data for Cycle 26. Match-ups between SLSTR and *in situ* data are provided by the EUMESAT OSI-SAF.

4.1 Dependence on latitude, TCWV, Satellite ZA and date

- The dependence of the difference between SLSTR SST_{skin} and drifting buoy SST_{depth} for Cycle 26 is shown in Figure 13. No adjustments have been made for difference in depth or time between the satellite and in situ measurements. SLSTR SSTs are extracted from the SL_2_WCT files. Daytime 2-channel (S8 and S9) results are shown in red, night time 2-channel results are shown in blue and night time 3-channel results are shown in green. Solid lines indicate dual-view retrievals, dashed lines indicate nadir-only retrievals. Bold lines indicate statistically significant (95% confidence) results.

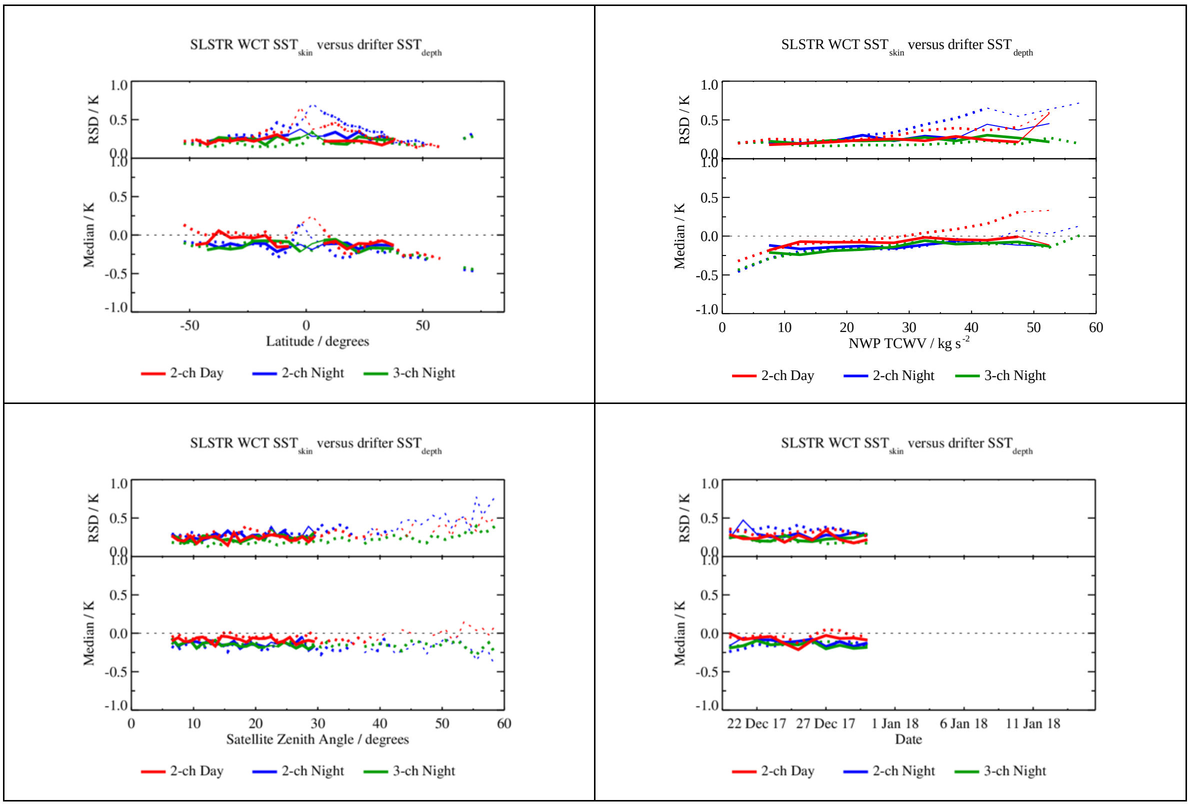

Figure 13: Dependence of median and robust standard deviation of match-ups between SLSTR SST_{skin} and drifting buoy SST_{depth} for Cycle 26 as a function of latitude, total column water vapour (TCWV), satellite zenith angle and date. The data gaps throughout the cycle are due to delays in match-up production.

4.2 Spatial distribution of match-ups

- The spatial distribution of SLSTR/drifter match-ups for Cycle 26 is shown in Figure 14. No adjustments have been made for difference in depth or time between the satellite and *in situ* measurements.

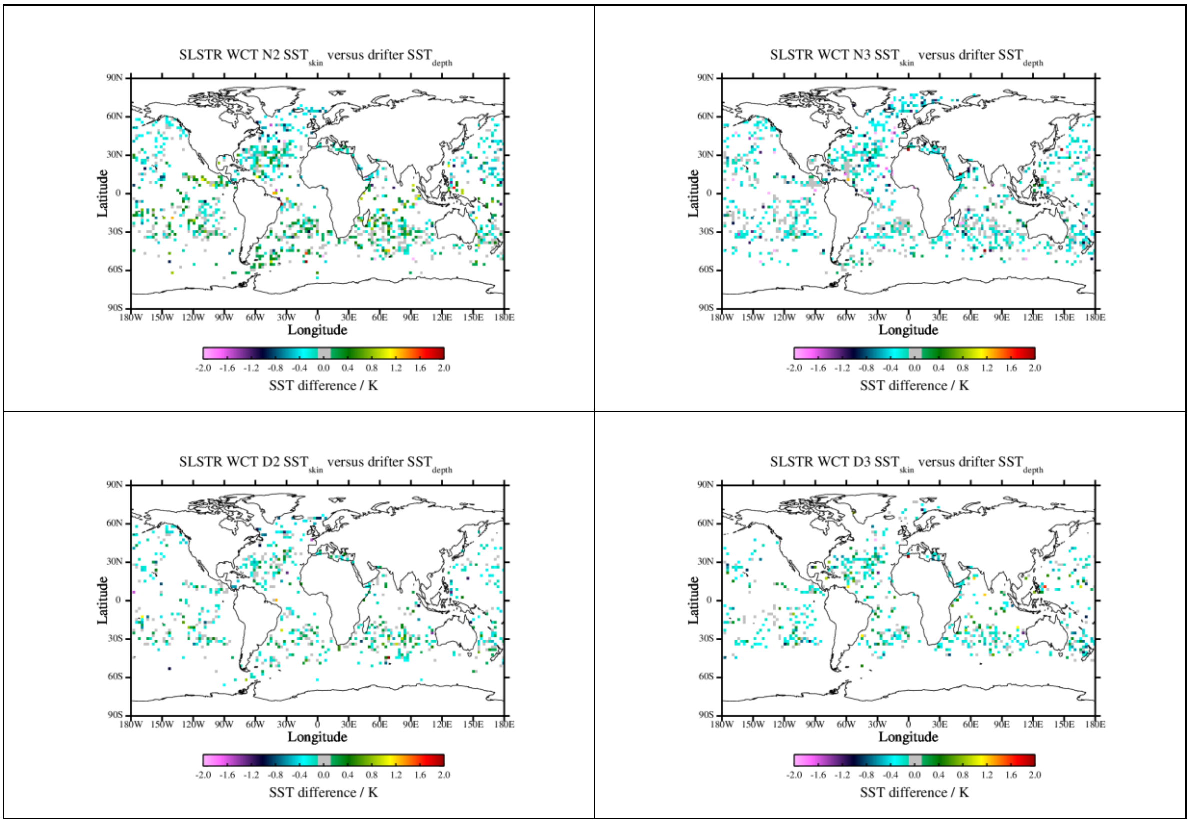

Figure 14: Spatial distribution of match-ups between SLSTR SST_{skin} and drifting buoy SST_{depth} for Cycle 26.

4.3 Match-ups statistics

- Match-ups statistics (median and robust standard deviation, RSD) of SLSTR/drifter match-ups for Cycle 26 are shown in Table 5. No adjustments have been made for difference in depth or time between the satellite and *in situ* measurements and so at night time (in the absence of diurnal warming) an offset of around -0.17 K is expected. The RSD values indicate SLSTR is providing SSTs mostly within its target accuracy (0.3 K).

Table 5: SLSTR drifter match-up statistics for Cycle 26.

Retrieval	Number	Median (K)	RSD (K)
N2 day	3152	-0.05	0.31
D2 day	1451	-0.09	0.24
N2 night	3651	-0.17	0.34
N3 night	3651	-0.15	0.21
D2 night	1398	-0.13	0.27
D3 night	1398	-0.15	0.24

5 Level 2 LST validation

Level 2 Land Surface Temperature products have been validated against *in situ* observations (Category-A validation), and intercompared (Category-C validation) with respect to three independent reference products from the ESA DUE GlobTemperature Project (MODIS, GOES, and SEVIRI).

5.1 Category-A validation

Category-A validation uses a comparison of satellite-retrieved LST with *in situ* measurements collected from radiometers sited at a number of stations spread across the Earth, for which the highest-quality validation can be achieved. The results can be summarised as follows (see Figure 15 and Figure 16):

- Average absolute accuracy (vs. Gold Standard):
  - Daytime: 0.81K
  - Night-time: 1.07K

  This daytime accuracy meets the mission requirement of < 1K. The night-time accuracy is very close to this mission requirement. This also is in line with the GCOS climate requirements of 1 K accuracy.

- Average precision (vs. Gold Standard):
  - Daytime: 0.72K
  - Night-time: 1.21K

  While there is no Sentinel-3 mission requirement for precision, the daytime precision meets the GCOS climate requirement of 1K. The night-time accuracy is also very close to this climate requirement.

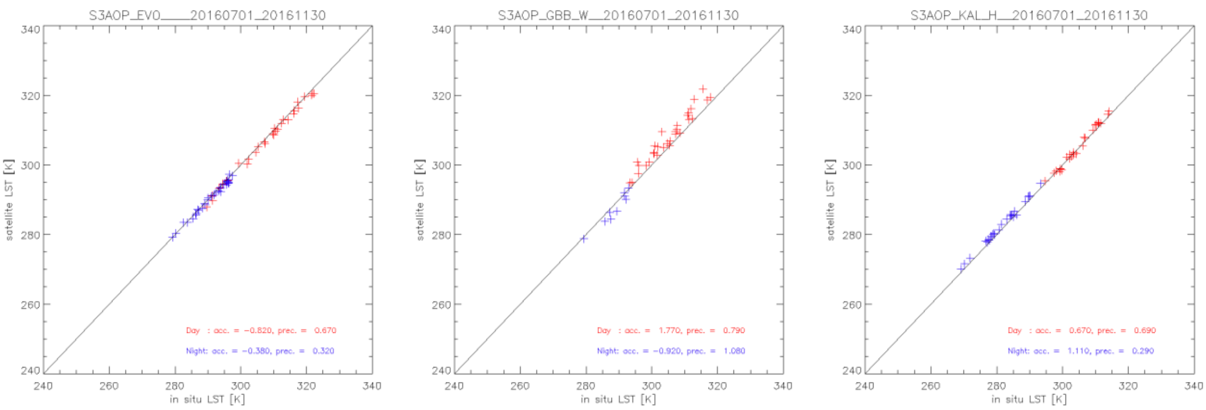

Figure 15: Validation of the SL_2_LST product over the mid-July to mid-November reprocessed period at three Gold Standard in situ stations managed by the Karlsruhe Institute of Technology: Evora, Portugal (left); Gobabeb, Namibia (centre); Kalahari-Heimat, Namibia (right). [Results courtesy of Maria Martin through the GlobTemperature Project]

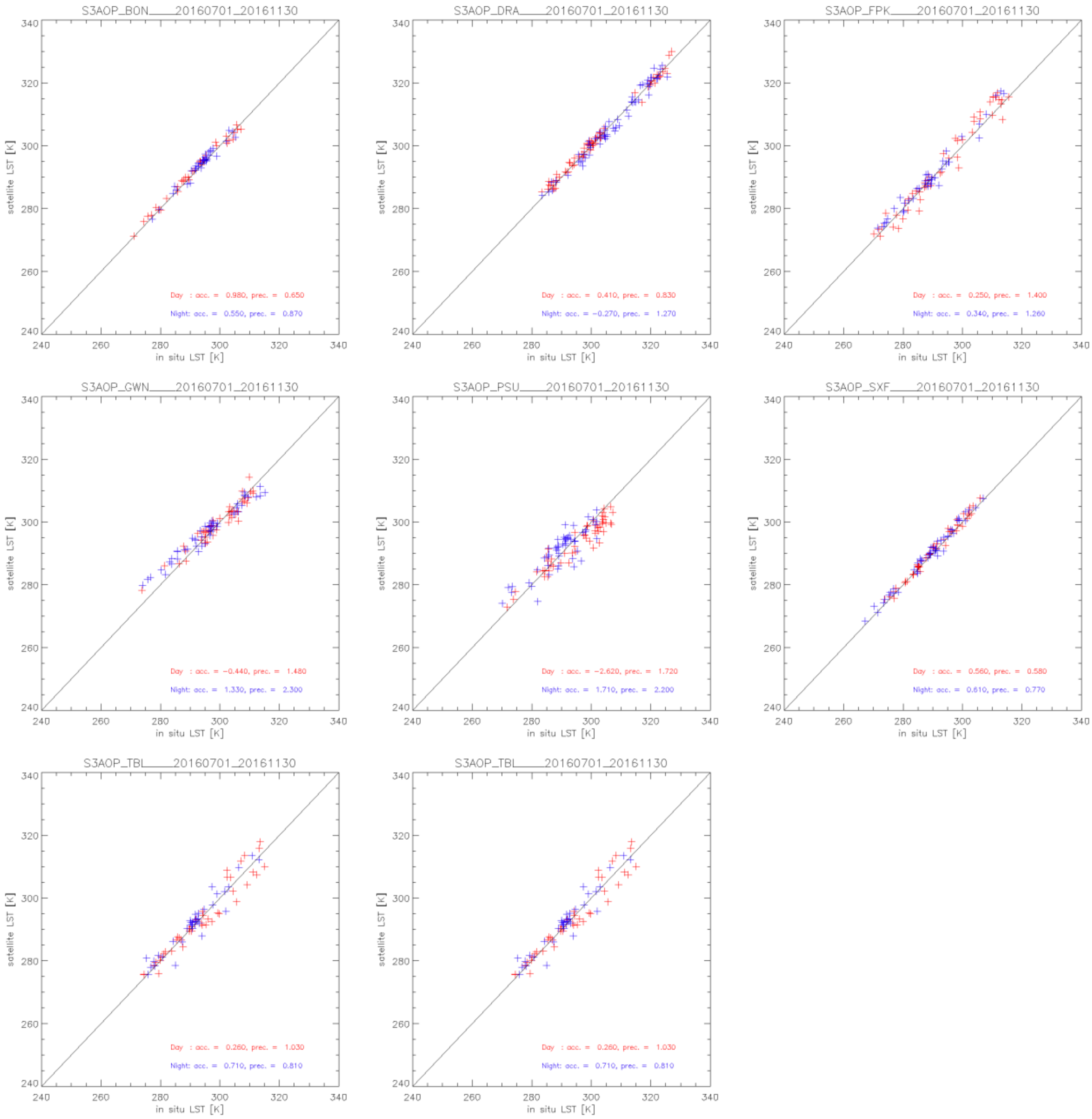

Figure 16: Validation of the SL_2_LST product over the mid-July to mid-November reprocessed period at the seven Gold Standard in situ stations of the SURFRAD network plus a Gold Standard station from the ARM network: Bondville, Illinois top-(left); Desert Rock, Nevada (top-centre); Fort Peck, Montana (top-right); Goodwin Creek, Mississippi (middle-left); Penn State University, Pennsylvania (middle-centre); Sioux Fall, South Dakota (middle-right); Table Mountain, Colorado (bottom-left); and Southern Great Plains, Oklahoma (bottom-centre).

5.2 Category-C validation

Category-C validation uses inter-comparisons with similar LST products from other sources such as AATSR, AVHRR, MODIS, SEVIRI, and VIIRS, which give important quality information with respect to spatial patterns in LST deviations. The results can be summarised as follows:

- Daytime intercomparison differences are: ~1K vs. GOES__LST_2 over North America; ~1K vs. SEVIR_LST_2 over Europe; and < 1K vs. MOGSV_LST_2 on a Global basis.
- Night-time intercomparison differences are: <1K vs. GOES__LST_2 over North America; <1K vs. SEVIR_LST_2 over Europe; and < 1K vs. MOGSV_LST_2 on a Global basis.
- Differences with respect to biomes tend to be larger during the day for surfaces with more heterogeneity and/or higher solar insolation. With respect to SLSTR zenith viewing angle differences are larger in the day on the left side of the SLSTR swath in the along-track direction.

6 Events

SLSTR was switched on and operating nominally during the cycle, with SUE scanning and autonomous switching between day and night modes.

However, there an issue with the Svalbard antenna on 1st January 2018, which caused a gap in the data received. This affects Level-1 and Level-2 product granules between 03:27 and 05:23, which show missing data (see Figure 17).

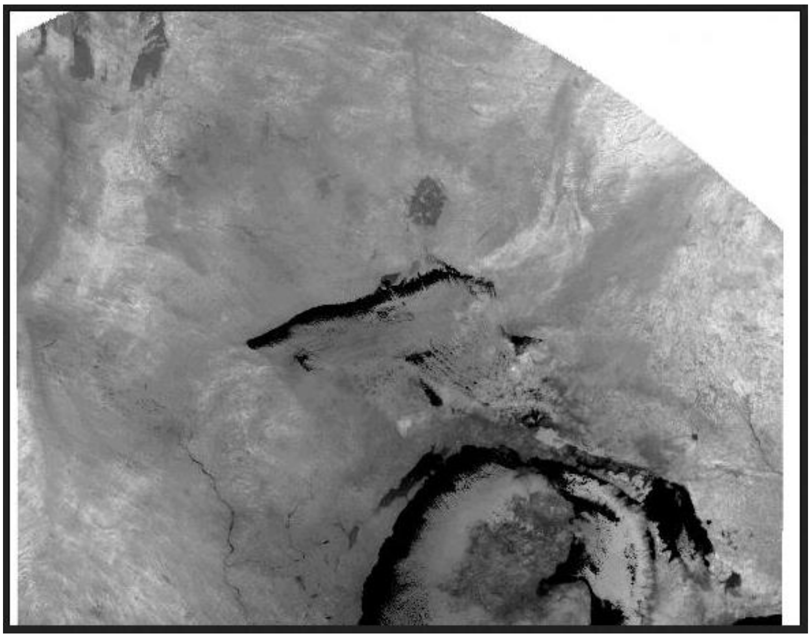

Figure 17: The quicklook image for the granule observed between 03:27 and 03:30 on 1st January 2018, showing the start of the missing data.

7 Appendix A

Other reports related to the Optical mission are:

- S3-A OLCI Cyclic Performance Report, Cycle No. 026 (ref. S3MPC.ACR.PR.01-026)

All Cyclic Performance Reports are available on MPC pages in Sentinel Online website, at: https://sentinel.esa.int

End of document